Transfer Learning Based Online Impedance Identification for Modular Multilevel Converters

Mengfan Zhang, *Member, IEEE*, Yang Zhang, *Member, IEEE*, and Qianwen Xu, *Member, IEEE*

***Abstract*—The large integration of modular multilevel converters (MMC) has introduced stability issues. The impedance-based stability analysis method is widely adopted, where the impedance model can be directly achieved at the terminals through nonintrusive measurement, which facilitates the black-box stability analysis of the MMC–grid interaction system. Yet, due to the limited impedance data amount in the practical application of online impedance identification, the accuracy of the identified model stability analysis cannot be guaranteed with existing methods in variable operating point scenarios. This article proposes a transfer learning based online impedance identification for MMC to address this research gap. The two-phase online impedance identification method is developed where the physical model of MMC in the offline phase is utilized to facilitate the online impedance identification. The proposed method can significantly reduce the data amount requirement in online impedance identification and achieve online stability analysis of the MMC system. The case studies confirm the effectiveness of the proposed method.**

***Index Terms*—Grid–converter interaction, impedance identification, modular multilevel converters (MMC,) stability, transfer learning.**

I. Introduction

MODULAR multilevel converters (MMC) have been widely adopted in high voltage DC (hvDC) transmission systems, electrical railway traction systems, and other medium voltage systems due to the advantages of the scalability, high efficiency, and low distortion [1], [2], [3]. However, the interaction between the internal dynamics of MMC (e.g., phase current control loop, capacitor voltage fluctuations, circulating current control loop, and synchronization loop) and the outer systems could introduce stability issues [4], [5].

The impedance-based stability analysis method has proven to be effective and widely adopted to reveal the interactions between the MMC and outer systems [6], [7], [8]. As reported in [9], the harmonic state space based small signal impedance model of the MMC is derived considering the internal harmonic dynamics. With the derived MMC impedance model, the MMC–grid interaction system can be modeled as the grid-side and converter-side subsystems, and the general Nyquist criterion (GNC) is adopted to judge the interaction stability by analyzing the impedance ratio of the subsystems [10], [11], [12]. Yet, in practical applications, the detailed parameters and structure of MMC are hard to be obtained from vendors. The impedance measurement based methods are the promising solutions to achieve the black box stability analysis of the system, which adopts the nonintrusive measurement at the terminal to obtain the impedance of the converter system [13], [14].

Considering the fluctuations and uncertainties of renewable generation and loads in the modern power system, it is essential to achieve the online impedance identification of MMC with variable operating points. As reported in [15], [16], and [17], the impedance measurement techniques are adopted for different topologies, which could achieve the gray-box or black-box modeling without detailed knowledge. A gray small-signal modeling method was proposed in [18], which adopted the particle-known knowledge to identify the control parameters of the converter system. Yet this method could not enable the black-box modeling of the system. An impedance identification method was reported in [19] for the voltage source converters (VSCs) with wide operating conditions, but it was limited to a known two-level VSC structure with a specific control structure, while it was not straightforwardly extended to MMC systems. Moreover, a system identification method was proposed in [20] for the dc-side impedance estimation of an MMC. Yet, the system topology and partial control system should be known, which could not enable the black-box modeling and degrade the effectiveness of the method in real-world applications.

To achieve online impedance identification at variable operating points in practical application, artificial neural network (ANN)-based methods were proposed in [21] and [22]. As reported in [21], the ANN-based impedance model is established, which can accurately generate the impedance at variable operating points. Yet, the ANN-based mission is data-hungry, which is not suitable for online impedance identification scenarios. To address the inherent data-hungry issue of neural network training, the physical-informed neural network based impedance identification method was proposed in [23], the physical knowledge of VSC was used to compress the neural network structure, which could largely reduce the training load of impedance model. Yet, this method requires the relationship between the operating point and impedance can be explicitly expressed, which can not be achieved in the MMC systems. Different from traditional two-level converters, the internal dynamics of the MMC will introduce harmonics to the system, which makes

Manuscript received 31 March 2023; revised 29 June 2023; accepted 19 July 2023. Date of publication 26 July 2023; date of current version 1 September 2023. This work was supported by Swedish Research Council (VR) Starting under Grant 2021-04434. Recommended for publication by Associate Editor T. Xu. *(Corresponding author: Qianwen Xu.)*

The authors are with the Electrical Power and Energy Systems Division, KTH Royal Institute of Technology, 114 28 Stockholm, Sweden (e-mail: mezhang@kth.se; zhang5@kth.se; qianwenx@kth.se).

Color versions of one or more figures in this article are available at https://doi.org/10.1109/TPEL.2023.3299194.

Digital Object Identifier 10.1109/TPEL.2023.3299194

the impedance model of the MMC nonlinearly relies on the operating point. The operating point-dependent characteristics make the practical application of online impedance identification time-consuming. Thus, the limited data amount in impedance identification of MMC could consequently affect the accuracy of the model and the stability analysis of the MMC–grid interaction system.

This article attempts to fill this research gap by proposing a transfer learning based online impedance identification method. The key idea is to utilize the physics of MMC in the offline phase to facilitate the online impedance identification of MMC. The proposed method consists of offline data generation and online impedance identification. First, the offline dataset is generated with the derived analytical model of the offline MMC, then the offline impedance model is generated by feeding the offline data. Second, the online impedance data is field-measured with the frequency scanning techniques, and then, by feeding the generated online data into the offline trained model with the transfer learning technique, the online impedance identification of MMC is achieved. The proposed method can achieve online impedance identification of MMC and stability analysis of the MMC–grid interaction system.

The rest of this article is organized as follows. The overall framework of the proposed transfer learning based online impedance identification of MMC is illustrated in Section II. Section III shows the detailed implementation of the proposed method, where the offline impedance model training and transfer learning based online impedance identification are illustrated. The case studies are provided in Section IV, where the experiment results can validate the effectiveness of the proposed method. Finally, Section V concludes this article.

II. Framework of Proposed Transfer Learning Based Online Impedance Identification of MMC

The conventional impedance measurement methods require tons of data to achieve accurate identification for the MMC impedance, thus they are time-consuming and cannot achieve online impedance identification. This article proposes a transfer learning based online impedance identification method to address this issue. The key idea is to use the analytical model of a standard MMC for offline training, to achieve the online identification of a real-world MMC through the designed transfer learning method. Then, only limited online data are required, and online stability evaluation of the MMC–grid interaction system can be achieved. The whole framework of the proposed method is visualized in Fig. 1. The method is divided into the offline phase and the online phase.

In the offline phase, the analytical model of the standard MMC (i.e., MMC1) is derived. By changing the operating point of the model, the offline impedance data of MMC can be obtained. To be noticed here, different from the two-level voltage source inverter (VSI) model, once the operating point of the MMC system changes, the steady-state harmonics of the MMC model need to be recalculated, the calculation process will be illustrated in detail in the following analytical impedance modeling part in Section III-A. The obtained data are structured as the format of

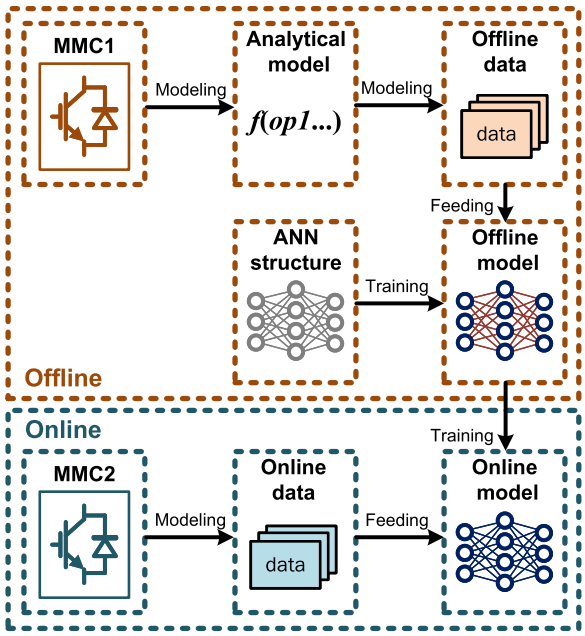

Fig. 1. Framework of the proposed transfer learning based online impedance identification method for MMC.

$\{input: op, f, output: Z_{MMC}(op, f)\}$, where op represents the operating point of the system, f represents the sweeping frequency, $Z_{MMC}(op, f)$ is the corresponding impedance of MMC. Then after the normalization, the dataset is prepared. By feeding the data into the designed ANN and training, the offline impedance model of MMC is generated.

In the online phase, the field test of impedance measurement of the real-world MMC (i.e., MMC2) is conducted, where the frequency scanning impedance measurement technology is adopted, as it can provide the highest signal-to-noise ratio (SNR) compared to other nonparametric impedance measurement methods [24]. By changing serval operating points of the MMC system, the online dataset can be obtained. The amount of online data are much smaller than the offline dataset. By feeding the online data into the trained offline model and training, the online impedance model of MMC2 can be generated.

The detailed implementation of the proposed transfer learning based online impedance identification of MMC is illustrated in the following Sections.

III. Implementation of the Proposed Method

The proposed method consists of the offline phase and online phase implementation, which are illustrated separately, as below. The key principle is to use the analytical model of a standard MMC for offline training, to achieve the online identification of a real-world MMC through the designed transfer learning method.

A. Offline Phase Training of a Standard MMC

In offline phase implementation, first, the analytical impedance model needs to be derived. The steady-state harmonics of the MMC system are highly related to the operation point.

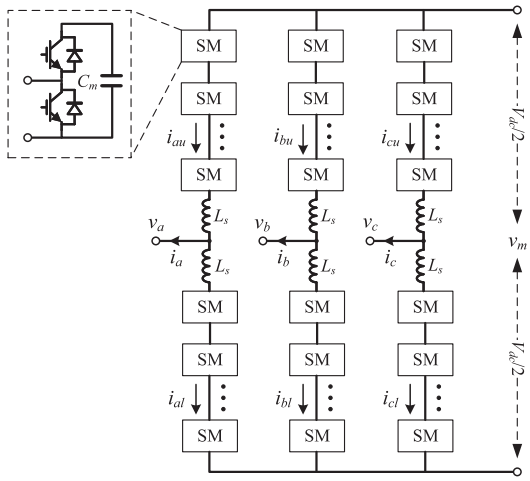

Fig. 2. Typical MMC topology.

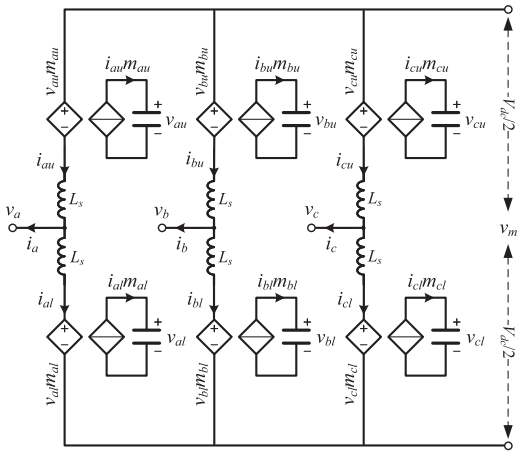

Fig. 3. Equivalent diagram of the typical MMC topology.

Thus, the steady-state harmonics need to be calculated with iteration. With the obtained harmonics, the analytical impedance model of a standard MMC can be derived. Then, the offline impedance dataset can be generated with the derived analytical model. By feeding the offline data and training, the offline impedance model can be obtained.

1) Analytical Modeling of MMC: The diagram of the three-phase MMC topology is shown in Fig. 2, where L_s is the arm inductor and C_m is the module capacitor. i_{xy}, i_x, and v_x represent the arm currents, output currents, and terminal voltages, respectively, where $x = a, b, c$ represents three phases and $y = u, l$ represents the upper and lower arms. $V_{\rm dc}$ represents the voltage of dc bus and v_m represents the voltage from the floating point of the dc bus to the ac neutral. As discussed in [7], the voltage balancing control of MMC does not have effects on the converter dynamics below the switching frequency, so the voltage of each module is assumed as the same. Thus, all the SMs in each upper/lower arm of MMC can be equivalent to one SM with N module capacitors in series. The equivalent circuit diagram of MMC can be represented as shown in Fig. 3, where v_{xy} and m_{xy} ($x = a, b, c$, $y = u, l$) represent the equivalent module voltages and modulation signals, respectively. Due to the common-mode and differential-mode characteristics of harmonic components, the impedance model of MMC can be obtained by modeling the upper or lower arm [7]. In this article, take the modeling of the upper arm in phase a as an example, the corresponding arm current and module voltage dynamics are modeled as follows:

$$\begin{aligned} L_s\frac{di_{\rm u}}{dt} &= \frac{1}{2}V_{dc} - v - v_{\rm u}m_{\rm u} + v_m \\ C\frac{dv_{\rm u}}{dt} &= i_{\rm u}m_{\rm u} \end{aligned} \tag{1}$$

where C represents the equivalent capacitance of each arm ($C = C_m/N$). The variables in (1) are extended to vectors to include the effects of nth harmonics in MMC, then the frequency domain model of corresponding arm current and module voltage dynamics can be represented as follows:

$$\begin{aligned} \mathbf{Z}_{l0}\mathbf{i}_u &= \frac{1}{2}V_{dc} - \frac{1}{2}\mathbf{v} - \mathbf{m}_u \otimes \mathbf{v}_u + \mathbf{v}_m \\ \mathbf{Y}_{c0}\mathbf{v}_u &= \mathbf{m}_u \otimes \mathbf{i}_u \end{aligned} \tag{2}$$

where $\otimes$ represents the convolution calculation, $\mathbf{i}_u$, $\mathbf{v}$, $\mathbf{m}_u$, $\mathbf{v}_u$, and $\mathbf{v}_m$ are harmonic vectors with $2n+1$ elements for arm current, terminal voltage, modulation signal, equivalent module voltage, and voltage from floating point to ac neutral, consisting of their complex Fourier coefficients in the order of frequency: $-nf_1$,..., $-f_1$, 0, f_1,..., nf_1. $\mathbf{Z}_{l0}$ and $\mathbf{Y}_{c0}$ are the impedance matrix of the inductance and admittance matrix of the capacitor, which can be written as follows:

$$\begin{aligned} \mathbf{Z}_{l0} &= j2\pi L_s \cdot diag[-nf_1, -(n-1)f_1, \ldots, \\ &\quad -f_1, 0, f_1, (n-1)f_1, nf]. \\ \mathbf{Y}_{c0} &= j2\pi C \cdot diag[-nf_1, -(n-1)f_1, \ldots, \\ &\quad -f_1, 0, f_1, (n-1)f_1, nf_1] \end{aligned} \tag{3}$$

where f_1 is the fundamental frequency. Considering the coupling between upper and lower arms operation and current control of the system (i.e., the output control and circulating current control), the steady-state harmonics can be calculated through the iteration of (2). It is noticed that each time the operating point changes, the harmonics need to be calculated. With the harmonic linearization, the small-signal model can be written as follows:

$$\begin{aligned} \mathbf{Z}_l\mathbf{i}'_u &= -\mathbf{v}'_p - \mathbf{V}_u\mathbf{m}'_u - \mathbf{M}_u\mathbf{v}'_u + \mathbf{v}'_m \\ \mathbf{Y}_c\mathbf{v}'_u &= \mathbf{I}_u\mathbf{m}'_u + \mathbf{M}_u\mathbf{i}'_u \end{aligned} \tag{4}$$

where $\mathbf{i}'_u$, $\mathbf{v}'_p$, $\mathbf{m}'_u$, $\mathbf{v}'_u$, and $\mathbf{v}'_m$ represent small-signal vectors for arm current, perturbation voltage, modulation signal, equivalent module voltage, and voltage from floating point to ac neutral, with $2n+1$ small-signal harmonics in the order of frequency: $f_p - nf_1$,..., $f_p - f_1$, f_p, $f_p + f_1$,..., $f_p + nf_1$. $\mathbf{V}_u$, $\mathbf{M}_u$, and $\mathbf{I}_u$ are harmonic matrices extended from corresponding harmonic vectors by Toplitz transform [3]. $\mathbf{Z}_l$ and $\mathbf{Y}_c$ are diagonal matrices representing the impedance of the arm inductance and admittance of the equivalent module capacitance at small-signal

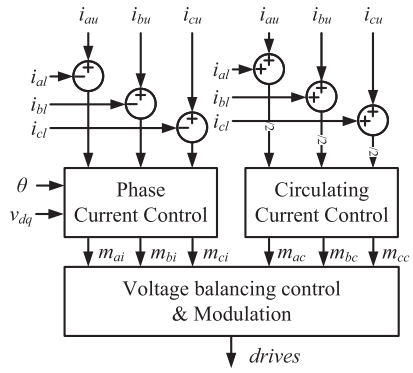

Fig. 4. Typical control diagram of MMC.

harmonic frequencies, expressed as

$$\begin{aligned}\mathbf{Z}_l &= j2\pi L_s \cdot diag[f_p - nf_1, f_p - (n-1)f_1, \ldots, \\ &\quad f_p - f_1, f_p, f_p + f_1, \ldots, f_p + (n-1)f_1, f_p + nf_1]. \\ \mathbf{Y}_c &= j2\pi C \cdot diag[f_p - nf_1, f_p - (n-1)f_1, \ldots, \\ &\quad f_p - f_1, f_p, f_p + f_1, \ldots, f_p + (n-1)f_1, f_p + nf_1].\end{aligned} \tag{5}$$

By analyzing the phase and sequence of small-signal harmonics, (4) can be simplified by forcing differential mode zero sequence currents to zero to eliminate $\mathbf{v}'_m$, thus, the (4) can be expressed as follows:

$$\begin{aligned}\mathbf{i}'_u &= -\mathbf{Y}_l(\mathbf{v}'_p + \mathbf{V}_u\mathbf{m}'_u + \mathbf{M}_u\mathbf{v}'_u) \\ \mathbf{v}'_u &= \mathbf{Z}_c\left(\mathbf{I}_u\mathbf{m}'_u + \mathbf{M}_u\mathbf{i}'_u\right)\end{aligned} \tag{6}$$

where $\mathbf{Z}_c = \mathbf{Y}_c^{-1}$ and $\mathbf{Y}_l$ can be calculated as follows:

$$\begin{aligned}\mathbf{Y}_l = diag\Bigg[\ldots, 0, &\frac{1}{j2\pi(f_p - 3f_1)L}, \ldots, \\ &\frac{1}{j2\pi f_p L}, \frac{1}{j2\pi(f_p + f_1)L}, 0, \\ &\frac{1}{j2\pi(f_p - 3f_1)L}, \ldots\Bigg].\end{aligned} \tag{7}$$

The typical control diagram of the MMC is shown in Fig. 4, which consists of phase current control, circulating current control, phase-locked loop (PLL), voltage feedforward control, and voltage balancing control. The phase current and PLL use the PI controller and the circulating current is controlled with the PR controller, which can be written as follows:

$$\begin{aligned}H_i(s) &= K_{pi} + \frac{K_{ii}}{s} \\ H_c(s) &= K_{pc} + \frac{2K_{rc} \cdot \omega_i s}{s^2 + 2\omega_i s + \omega_n^2} \\ H_\theta(s) &= K_{ppll} + \frac{K_{ipll}}{s}\end{aligned} \tag{8}$$

where $H_i(s)$, $H_c(s)$, and $H_\theta(s)$ are the transfer functions of phase current control and circulating current control, respectively. K_{pi}, K_{ii}, K_{pc}, K_{rc}, K_{ppll}, and K_{ipll} are the corresponding proportional gain, integral gain, and resonant gain. Based on [7], the small-signal control model of MMC without considering the voltage balancing control can be expressed as follows:

$$\mathbf{m}'_u = (\mathbf{Q}_i + \mathbf{Q}_c) \cdot \mathbf{i}'_u + (\mathbf{P} + \mathbf{F}) \cdot \mathbf{v}'_p \tag{9}$$

where $\mathbf{Q_i}$ and $\mathbf{Q_c}$, representing the gain of phase current control and circulating current control, are the $2n+1$ order diagonal matrices. The corresponding elements in the matrices are written as follows:

$$\begin{aligned}q_i = \{&H_i\left(j2\pi\left(f_p + kf_1\right) - [\bmod(k+2,3) - 1]j2\pi \cdot f_1\right)\} \\ &\cdot \frac{1 + (-1)^k}{2} \cdot |\bmod(k+2,3) - 1|\end{aligned} \tag{10}$$

$$q_c = H_c\left(j2\pi\left(f_p + kf_1\right)\right) \cdot \frac{1 + (-1)^k}{2} \tag{11}$$

where mod represents the modulo calculation and $k = -n, \ldots, 0, \ldots, n$. The gain of PLL can be represented using a $2n+1$ order matrix $\mathbf{P}$, where the $(n-1, n+1)$-th and $(n+1, n+1)$-th elements are represented as follows:

$$\frac{\mathbf{M}_1 - \mathbf{I}_1 H_i\left(j2\pi\left(f_p - f_1\right)\right)}{2} \cdot G_\theta\left(j2\pi\left(f_p - f_1\right)\right) \tag{12}$$

$$\frac{\mathbf{I}_1 H_i\left(j2\pi\left(f_p - f_1\right)\right) - \mathbf{M}_1^*}{2} \cdot G_\theta\left(j2\pi\left(f_p - f_1\right)\right) \tag{13}$$

where $G_\theta(s) = H_\theta(s)/(s + V_1 H_\theta(s))$ represents the gain of PLL, V_1 represents the magnitude of the grid voltage of the MMC system, $\mathbf{M}_1$ and $\mathbf{I}_1$ are the frequency-domain fundamental phasor of modulation signal and phase current. The other elements are all zero. On the other hand, the gain of voltage feedforward can also be represented using a $2n+1$ order matrix $\mathbf{F}$, where the $(n-1, n+1)$-th and $(n+1, n+1)$-th elements are represented as follows:

$$-\frac{V_1}{2} \cdot G_\theta\left(j2\pi\left(f_p - f_1\right)\right) \tag{14}$$

$$-1 + \frac{V_1}{2} \cdot G_\theta\left(j2\pi\left(f_p - f_1\right)\right). \tag{15}$$

Finally, the small-signal responses of the upper arm current to a perturbation voltage can be modeled by the admittance coefficient matrix, expressed as follows:

$$\begin{aligned}\mathbf{Y} = &[\mathbf{U} + \mathbf{Y}_l\mathbf{M}\mathbf{Z}_c\mathbf{M} + \mathbf{Y}_l(\mathbf{V} + \mathbf{M}\mathbf{Z}_c\mathbf{I})(\mathbf{Q}_i + \mathbf{Q}_c)]^{-1} \\ &\cdot \mathbf{Y}_l[\mathbf{U} + (\mathbf{V} + \mathbf{M}\mathbf{Z}_c\mathbf{I})(\mathbf{P} + \mathbf{F})]\end{aligned} \tag{16}$$

where $\mathbf{U}$ is the $2n+1$ order identity matrix. Since the phase current at f_p and $f_p - 2f_1$ are twice the arm current, the impedance of MMC can be expressed as follows [25]:

$$Y_{MMC}\left(f_p\right) = \begin{bmatrix} Y_{11}\left(f_p\right) & Y_{12}\left(f_p\right) \\ Y_{21}\left(f_p\right) & Y_{22}\left(f_p\right) \end{bmatrix}$$

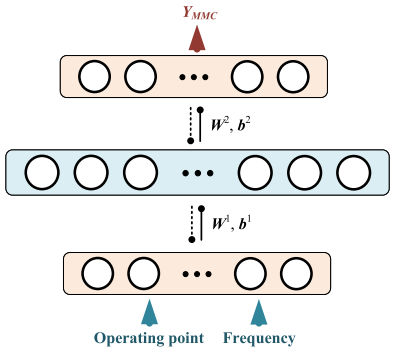

Fig. 5. Structure diagram of three-layer feedforward neural network.

$$= \begin{bmatrix} Y_p^*(2f_1 - f_p) & Y_c(f_p) \\ Y_c^*(2f_1 - f_p) & Y_p(f_p) \end{bmatrix} \quad (17)$$

where Y_{sp}, Y_{sc} are the $(n+1, n+1)$-th element, the $(n-1, n+1)$-th element of $\mathbf{Y}$, respectively. With the derived impedance model of MMC, the dataset can be generated.

2) Offline Impedance Model Training: The derived model could generate the data of the impedance model of MMC. Then, the obtained data are structured as the format of $\{input : op, f, output : Y_{MMC}(op, f)\}$. Here, the generated admittance data are very small numerically, so in this article, the magnitude and phase are used to represent the admittance of MMC. Then, after the normalization, the dataset is prepared.

For the ANN training, the first step is to choose the neural network structure. The impedance identification is to establish the map between the pair of frequency and operating points and the corresponding admittance of MMC. As the relationship between them is static, the feedforward neural network is selected in this article. The next step is to design the structure of the feedforward neural network. As the mapping between frequency and operating points and the corresponding admittance of MMC are continuous and surjective, the single hidden layer is sufficient to capture the characteristics of this mapping. Therefore, a three-layer feedforward neural network as shown in Fig. 5, which consists of one hidden layer, one input layer, and one output layer, is adopted in this article, where each layer consists of a different number of neurons. The numbers of neurons in the input layer and output layer are dependent on the structure, while the number of neurons in the hidden layer needs trial and error. In this article, the neuron number in the hidden layer is 128. And for the jth neuron in different layers, the output can be represented as follows:

$$y_j = A\left[\sum_{i=1}^{k}\left(w_{i,j}^{1or2} \cdot x_i\right) + b_j^{1or2}\right]|_{j=1,\ldots,m} \quad (18)$$

where x_i is the input of the neuron; w and b represent the weight and bias of the neuron, respectively; A represents the activation function. Since the shallow neural network structure is adopted in the article, the sigmoid function is selected as the activation function in the hidden layer to perceive the nonlinearity of the impedance model of MMC, while the linear function serves as the activation function in the output layer and input layer.

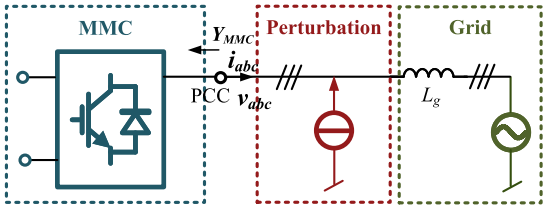

Fig. 6. Diagram of the online impedance measurement of MMC.

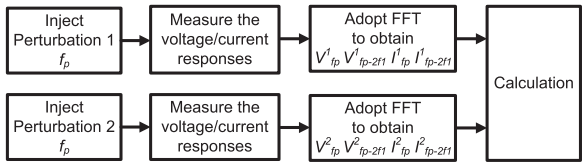

Fig. 7. Workflow of online impedance measurement of MMC.

The next step is the model training, the back-propagation algorithm is adopted to train the ANN model, while the mean squared error (MSE) between the neural network output and measured impedance data is selected as the loss function. The training process is to reduce the MSE by updating the weights and biases of each neuron. After the training, the offline impedance model of the MMC is obtained.

B. Online Identification of a Real-World MMC

In the online phase implementation, first the frequency scanning impedance measurement is adopted to obtain the online impedance data of a real-world MMC. Then, by feeding the field-measured impedance data into the offline impedance model and with the developed transfer learning technique, the online impedance model can be obtained.

Fig. 6 shows the diagram of the online impedance measurement of the MMC. The idea is to inject the small perturbation with designed frequency into the MMC to be measured, then sample the voltage and current response at the point of common coupling (PCC), with the calculation, the impedance of MMC at the corresponding operating point and frequency can be obtained. The detailed workflow is illustrated in Fig. 7.

The first step is to make the MMC works in a steady state with the given operation point $op1$. Then, the small signal current perturbation is injected into the system at the PCC. Here, the magnitude of the perturbation is to be designed to be small enough not to change the steady-state value of the operating point, but large enough to avoid the noise from the MMC operation. In this article, the magnitude is set to 2% of the steady-state value [26]. Considering the frequency coupling effect in the MMC model, the perturbation with frequency f_p could introduce a frequency response at frequency $f_p - 2f_1$, where f_1 is the fundamental frequency of the system. The twice perturbations are injected into the MMC system to obtain the second-order impedance matrix. Then, the voltage and current responses can be measured at PCC. With the help of the fast Fourier transform (FFT) algorithm, the corresponding responses at f_p and $f_p - 2f_1(V_{fp}, V_{fp-2f1}, I_{fp}, I_{fp-2f1})$ can be obtained. Then, the admittance matrix of MMC at operating point $op1$ can

be calculated as follows:

$$Y(f_p) = \begin{bmatrix} V_{fp}^1 & V_{fp}^2 \\ V_{fp-2f1}^1 & V_{fp-2f1}^2 \end{bmatrix}^{-1} \begin{bmatrix} I_{fp}^1 & I_{fp}^2 \\ I_{fp-2f1}^1 & I_{fp-2f1}^2 \end{bmatrix}. \tag{19}$$

Repeating the frequency scanning by changing the frequency of the perturbation and the steady-state operating point of the MMC system, the admittance dataset can be established, where the structure of the dataset is the same as in the offline implementation phase and the data amount is much smaller than the offline dataset.

In transfer learning theory, the offline training is corresponding to the source domain, while the online impedance identification corresponds to the target domain, where the domain consists of a feature space of input I and the corresponding probability distribution $P(I)$. Denote the source domain data with $D_s = \{(i_{s1}, o_{s1}), \ldots, (i_{sn}, o_{sn})\}$, where the input I_s is the set of the steady state operating point of the standard MMC (MMC1) and corresponding frequency and Os is the set of corresponding output, i.e., the admittance model of the standard MMC (MMC1). Similarly in the target domain, the field-measured admittance data of the real-world MMC (MMC2) can be denoted with $D_t = \{(i_{t1}, o_{t1}), \ldots, (i_{tm}, o_{tm})\}$, where the data amount of the target domain is smaller than the source domain, i.e., $m < n$. If the data in the target domain follow the same distribution as the source and target domain, the transfer learning from the source domain to the target domain can achieve satisfactory accuracy [27]. In this article, the field-measured dataset and the offline training dataset follow the same distribution, thus, transfer learning could be easily achieved. In online training, the adaptive moment estimation (Adam) method is used as the optimization algorithm, as Adam can combine the benefits of both momentum-based optimization and adaptive learning rate methods and has been shown to perform well on a wide range of deep learning tasks [28], [29]. The training batch size is set to 128 in this article to yield a more stable estimate of the gradients.

Then, the field-measured impedance data are fed into the trained offline impedance model with the transfer learning technique and the online impedance model of the real-world MMC (MMC2) can be obtained.

IV. Case Study

To validate the proposed method, the case studies are designed in this section. The proposed method is adopted to identify the online impedance model of MMC with the phase control loop, voltage feedforward, circulating current control loop, voltage balancing loop, and PLL. The proposed transfer learning method is to use the knowledge of the offline MMC to help the training of the online MMC. Thus, in the case study, the offline MMC is marked as MMC1 while the online MMC is marked as MMC2. The detailed parameters of the MMCs are listed in Table I. According to the setup of the case study, the online MMC2 is a black-box system, only the nonintrusive measurement is allowed. To show the effectiveness of the proposed transfer learning based impedance identification method, the first case study is designed to show the accuracy of obtained impedance model of MMC and the advantages against the conventional ANN-based impedance identification method. The second case study is designed to show the application of the proposed method in the practical stability analysis of the MMC–grid interaction system.

TABLE I
MMC Parameters

Variables	MMC1 Value	MMC2 Value
V_{dc}	700 V	800 V
f_1	50 Hz	50 Hz
f_s	20 kHz	10 kHz
L_s	2.5 mH	5 mH
C_m	0.26 mF	0.26 mF
K_{pi}	2.8	10
K_{ii}	324	324
K_{pc}	2.5	5
K_{rc}	300	600
K_{ppll}	1	0.05
K_{ipll}	320	198
n	2	2

A. Accuracy Validation and Comparison Against the Conventional ANN-Based Impedance Identification

Considering the two MMC systems shown in Table I, the MMC2 is a black-box system while the MMC1 is known. Following the workflow of the proposed transfer learning based online impedance identification method, the impedance model of the offline MMC1 is generated with the data generated by the derived analytical model in Section II. To easily visualize the results, only the current is selected as the variable operating point. The online field-measured impedance data of MMC2 are visualized as shown in Fig. 8, where the frequency f_p varies from 1 to 200 Hz with the 10-Hz interval, and the current I varies from 1 to 30 A with 2 A interval. Then feed the measured admittance dataset into the trained offline admittance model of the MMC2, with the transfer learning technique the online admittance model of the MMC2 is obtained, which is visualized as shown in Fig. 9.

To show the effectiveness of the proposed method against the conventional ANN method, the corresponding errors between the trained admittance model with the proposed method and the conventional ANN method are shown in Figs. 10 and 11. The model error of the existing ANN-based method is much larger (around 10 times). From the comparison between the corresponding errors, the conventional ANN-based method cannot achieve good performance in online small data scenarios, while the proposed method can guarantee accuracy even with the small data amount.

B. Applied in Practical Stability Analysis of the MMC–Grid Interaction System

The generated impedance model of MMC using the proposed transfer learning based online impedance identification can be used in stability analysis of the interaction system of the MMC and grid, which is shown in Fig. 12. The generalized Nyquist criterion (GNC) is used to analyze the interaction system by analyzing the eigenlocus of the equivalent transfer function. The

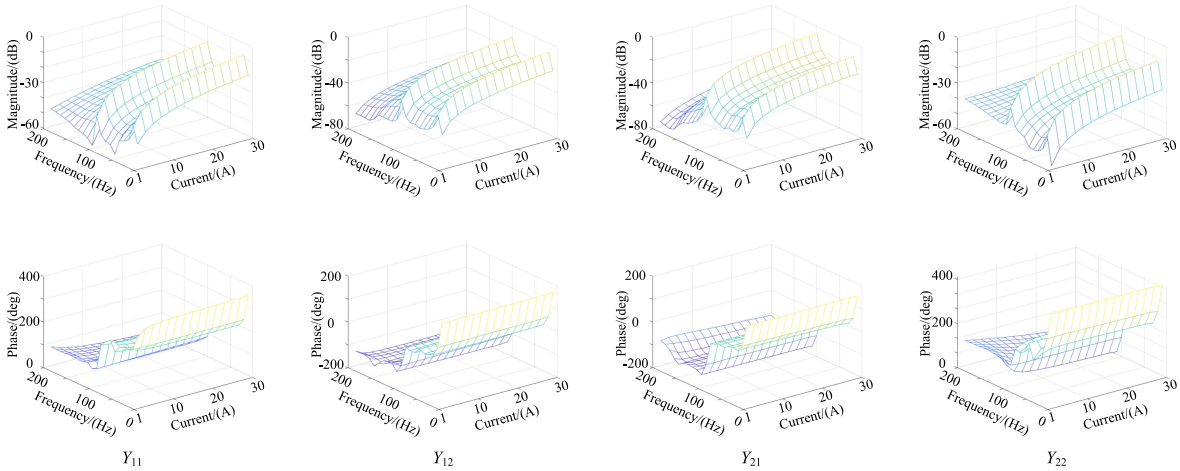

Fig. 8. Measured admittance of MMC2.

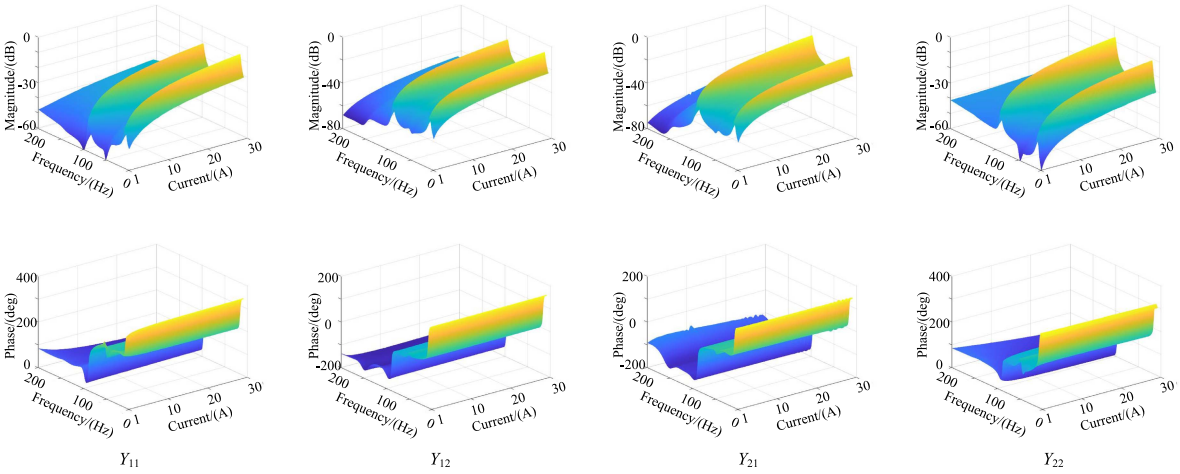

Fig. 9. Trained online admittance model of MMC2.

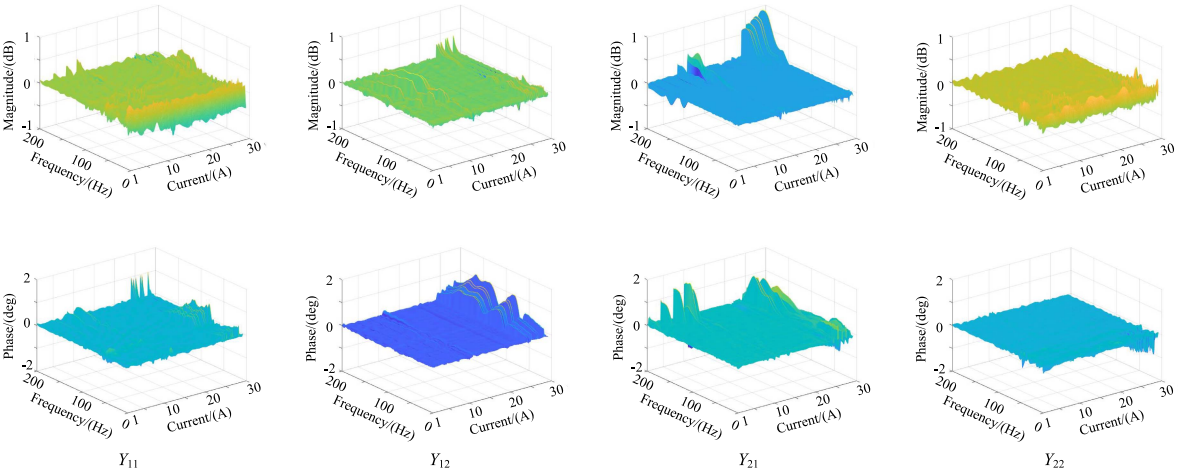

Fig. 10. Corresponding errors between trained admittance model using the proposed method and analytical admittance model.

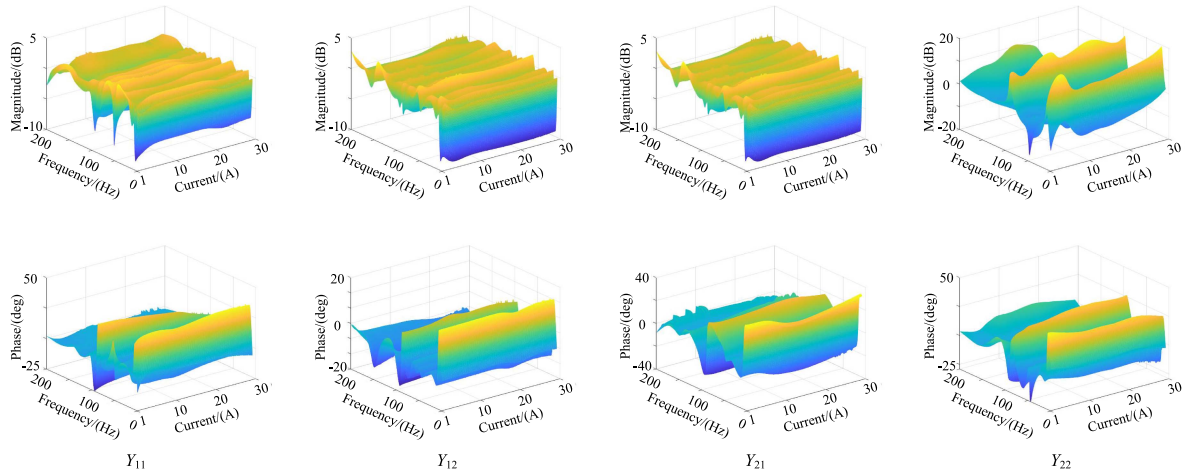

Fig. 11. Corresponding errors between trained admittance model using conventional ANN method and analytical admittance model.

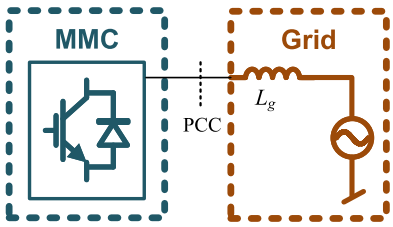

Fig. 12. Simplified diagram of grid–MMC interaction system.

TABLE II
STABILITY ANALYSIS RESULT

Symbol	Current	Voltage	Stability
a	4 A	230 V	Stable
b	7 A	230 V	Unstable
c	4 A	200 V	Unstable

parameters of MMC2 in the experiment are the same as shown in Table I. Three cases of different steady-state operating points are tested. When the grid inductor is 10 mH, the Nyquist diagram of the three cases is obtained as shown in Fig. 13. From the diagram, case I is stable while case II and case III are unstable; the result is shown in Table II. It is noticed that although they are both unstable, the system working at operating point b is more vulnerable at operating point c.

The corresponding experiment is conducted to validate the stability analysis result using the obtained MMC model. The diagram of the experiment setup is shown in Fig. 14. The Imperix power modules are used to build the MMC system, where each phase has four modular. The Chroma 61830 serves as the grid simulator and the Chroma 62120D is used for the dc power supply.

Three cases shown in Table II are tested, and the corresponding steady-state experimental results are shown in Fig. 15, where the V_{ga} is the voltage at PCC; I_a, I_b, I_c are the output current of MMC. As shown in the experimental results, when the interaction system operates with the operating point a, the system is stable, when the system operates with the operating points b and c, the system is unstable. The experiment results match

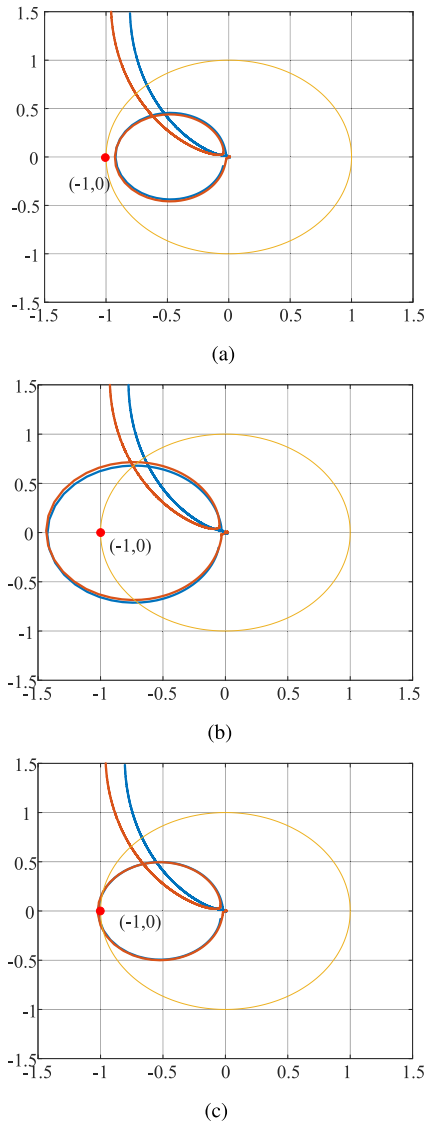

Fig. 13. Nyquist diagrams at different operation points of MMC–grid interaction system. (a) Case I. (b) Case II. (c) Case III.

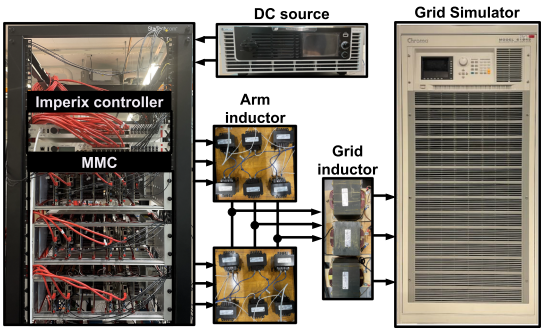

Fig. 14. Experiment setup.

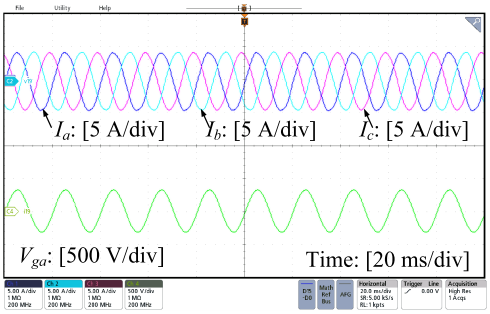

(a)

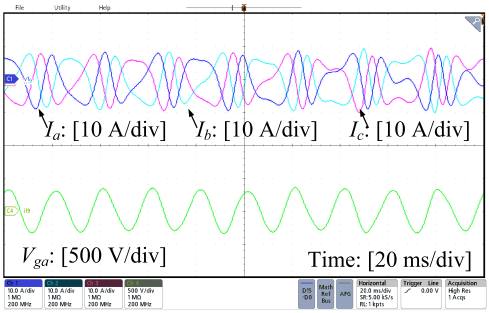

(b)

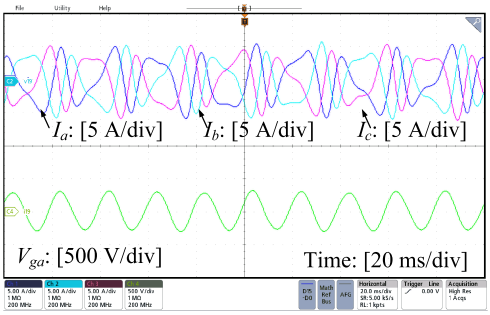

(c)

Fig. 15. Experimental results of MMC–grid interaction system at different operating points. (a) Case I: operating point a. (b) Case II: operating point b. (c) Case III: operating point c.

the corresponding stability analysis results using the trained impedance model of MMC. The transient processes of the operating point changing are shown in Fig. 16. In Fig. 16(a), the operating point is changing from operating point a to operating point b at t_1; then, the system becomes unstable and collapses at t_2. In Fig. 16(b), the operating point is changed to operating point c; then, the system becomes unstable and collapses at t_1.

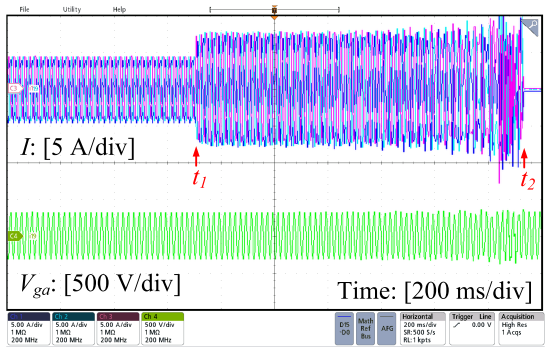

(a)

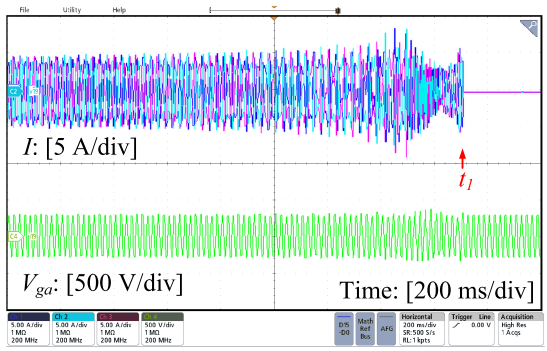

(b)

Fig. 16. Experimental results of MMC–grid interaction system at different operating points. (a) Case I: Transient process from operating point a to b. (b) Case II: Transient process of operating point c.

It is noticed that when the oscillation occurs in the system, the system working at operating point b takes more time to collapse than the operating point c, which shows that the system is more vulnerable than at operating point c, which also matches the stability analysis results as shown in Fig. 13. The experimental results validate the effectiveness of the obtained impedance model with the proposed method for stability analysis.

To compare the stability analysis performance of different impedance models identified with the conventional ANN method and the proposed transfer learning based method, we have checked the Nyquist diagram at different operating points with the conventional ANN method and the proposed method. Nyquist diagram at different operating points with the conventional ANN method is shown in Fig. 17. From the Nyquist diagram drawn with the conventional ANN model, when the interaction system operates at 4 and 7 A, the system will be stable. While the Nyquist diagram drawn with the proposed method is shown in Fig. 13, when the interaction system operates at 4 A, the system will be stable, and when the system operates at 7 A, the system will be unstable. When we check the experiment results shown in Fig. 15, for the two operating points, the experimental results show that system is stable when it operates at 4 A, and unstable when it operates at 7 A. Thus, the experiment results do not match the stability analysis results using the conventional ANN model, while the impedance model generated by the proposed method can give the correct stability analysis results validated by experimental results. Therefore, it demonstrates that the proposed transfer learning based online

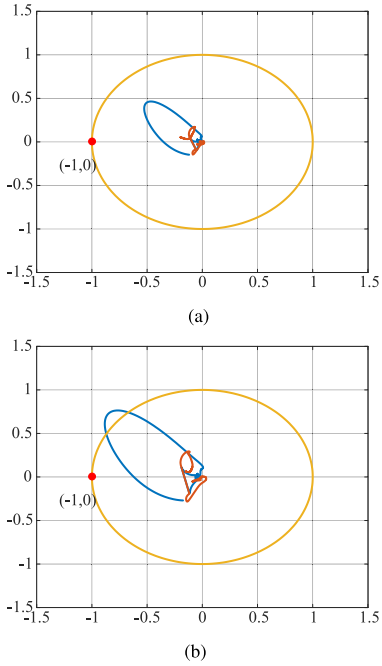

Fig. 17. Nyquist diagrams at different operation points of MMC–grid interaction system with conventional ANN model. (a). The operating current is 4 A. (b). The operating point is 7 A.

TABLE III
STABILITY ANALYSIS RESULT ($C_m = 1.04$ MF)

Symbol	Current	Voltage	Stability
a	4 A	230 V	Stable
b	7 A	230 V	Unstable

impedance identification method has better performance and higher accuracy in the stability analysis of MMC–grid interaction systems.

C. Applied in Practical Stability Analysis of the MMC–Grid Interaction System With Different Parameters

To show the effectiveness of the proposed method of the impedance identification of the MMC systems with different parameters, we have conducted experiments with different modular capacitors. Then, we conduct the experiment when the SM capacitors change to 1.04 mF while the other parameters of the MMC2 remain the same. After the impedance model of the MMC2 with 1.04 mF is generated with the proposed method, to further check the effectiveness of the generated impedance model in the stability analysis of the interaction system of MMC and grid, the GNC method is adopted to analyze the stability of interaction system by analyzing the eigenlocus of the equivalent transfer function. Two cases of different steady-state operating points are tested. When the grid inductor is 10 mH, the Nyquist diagram of the two cases is obtained as shown in Fig. 18. From the diagram, case I is stable while case II is unstable, the stability analysis result is shown in Table III.

The corresponding experiment is conducted to validate the stability analysis result using the obtained MMC impedance

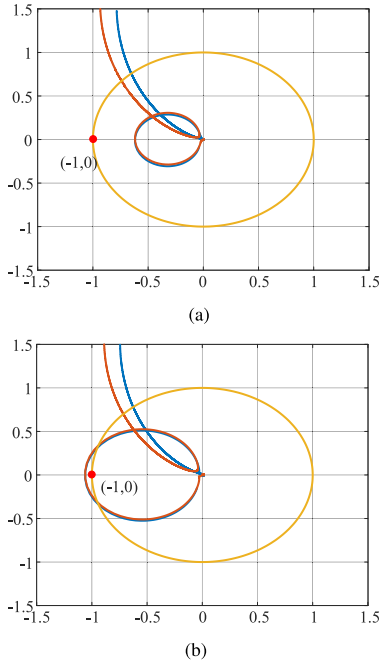

Fig. 18. Nyquist diagrams at different operation points of MMC–grid interaction system with 1.04 mF capacitor at different operating points. (a) Case I: operating point a. (b) Case II: operating point b.

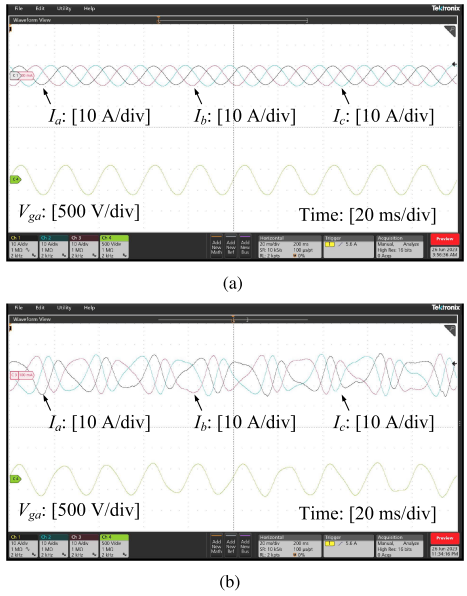

Fig. 19. Experimental results of the MMC–grid interaction system with 1.04 mF capacitor at different operating points. (a) Case I: operating point a. (b) Case II: operating point b.

model. Two cases shown in Table III are tested, and the corresponding steady-state experimental results are shown in Fig. 19, where the V_{ga} is the grid voltage, and I_a, I_b, I_c are the output current of the MMC. As shown in the experimental results, when the interaction system operates with the operating point a, the system is stable, when the system operates with the operating point b, the system is unstable. The experiment results match the stability analysis results using the trained impedance model of MMC. The transient processes of the operating point change are

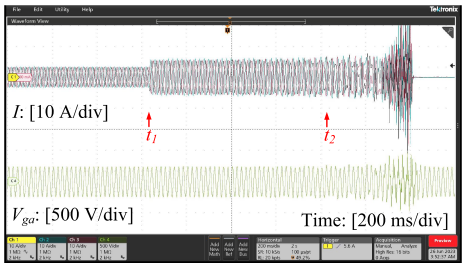

Fig. 20. Experimental results of the MMC–grid interaction system with 1.04 mF capacitor at different operating points: Transient process from operating point a to b.

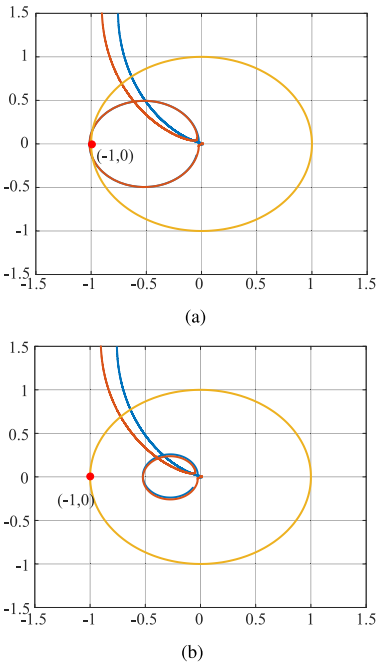

Fig. 21. Nyquist diagrams with different PLL parameters of MMC–grid interaction system. (a) The proportional gain of PLL k_{ppll} is 0.05. (b) The proportional gain of PLL k_{ppll} is 0.12.

shown in Fig. 20. In Fig. 20, the operating point is changing from operating point a to operating point b at t_1, then the oscillation occurs in the system, and then the system collapses at t_2. The experimental results validate the effectiveness of the obtained impedance model with the proposed method for stability analysis in the scenario when the parameters are different.

D. Applied in Stabilizing the MMC–Grid Interaction System

The trained admittance model of MMC could be used for stabilizing the MMC–grid interaction system. The trained MMC admittance model shown in Fig. 9 shows that there is a peak around 100 Hz. As discussed in [30], near-synchronous oscillations are usually caused by the PLL. Thus, we can stabilize the system by tuning the control parameters of PLL.

When the operating current of the MMC system is 6 A and the proportional gain of PLL k_{ppll} is 0.05, the Nyquist diagram is shown in Fig. 21(a), which shows the interaction system has oscillations and will be unstable. Then, we change the proportional gain of PLL k_{ppll} to 0.12, the Nyquist diagram

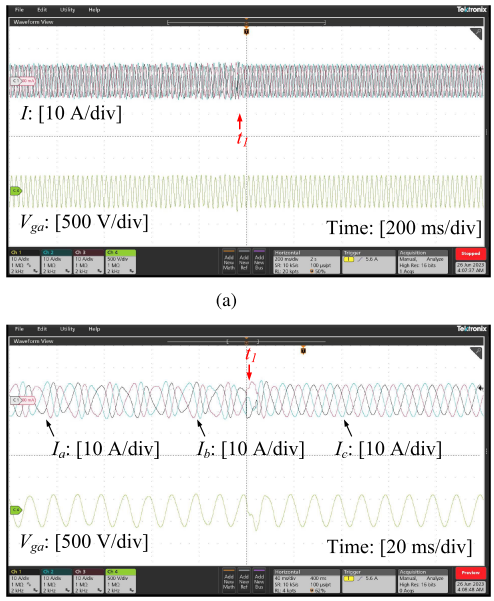

Fig. 22. Experimental results of MMC–grid interaction system with different control parameters. (a) Transient process when k_{ppll} changes from 0.05 to 0.12. (b) Zoom-in diagram of the transient process when k_{ppll} changes from 0.05 to 0.12.

changes as shown in Fig. 21(b), which means the interaction system will become stable. Then, the experiment is conducted to validate the stability analysis. The corresponding experiment results are shown in Fig. 22. The MMC system operates beginning with $k_{ppll} = 0.05$, while the operating current is 6 A. In the beginning, oscillation occurs in the interaction system, which matches the stability analysis result by the Nyquist diagram. Then, we change the k_{ppll} to 0.12 at time t_1, then after several switching periods, the system becomes stable. The transient process when k_{ppll} changes from 0.05 to 0.12 shows the effectiveness of stabilizing the MMC–grid interaction system using the identified admittance model generated by the proposed transfer learning based online impedance identification method.

V. Conclusion

This article proposes a transfer learning based online impedance identification method for MMC. Considering the data amount limitation in online impedance identification, the transfer learning based online impedance identification method is developed. The two-phase impedance identification is developed with the inspiration of the transfer learning theory to achieve effective online impedance identification. By making full use of the analytical physical model and data from a known offline MMC, the proposed method can enable an accurate online impedance identification of the MMC with different and unknown online MMC. The comparison results show that the proposed transfer learning based method has superiority over the conventional ANN-based methods. The experiment results can validate the effectiveness of the proposed method used for online impedance identification and stability analysis of the MMC–grid interaction system.

REFERENCES

[1] A. Nami, J. Liang, F. Dijkhuizen, and G. D. Demetriades, "Modular multilevel converters for HVDC applications: Review on converter cells and functionalities," *IEEE Trans. Power Electron.*, vol. 30, no. 1, pp. 18–36, Jan. 2015.

[2] J. Lyu, X. Cai, and M. Molinas, "Frequency domain stability analysis of MMC-based HVDC for wind farm integration," *IEEE Trans. Emerg. Sel. Topics Power Electron.*, vol. 4, no. 1, pp. 141–151, Mar. 2016.

[3] Y. Zhang, X. Chen, and J. Sun, "Sequence impedance modeling and analysis of MMC in single-star configuration," *IEEE Trans. Power Electron.*, vol. 35, no. 1, pp. 334–346, Jan. 2019.

[4] J. Lyu, X. Cai, M. Amin, and M. Molinas, "Sub-synchronous oscillation mechanism and its suppression in MMC-based HVDC connected wind farms," *IET Generation, Transmiss. Distrib.*, vol. 12, no. 4, pp. 1021–1029, 2018.

[5] H. Wu, X. Wang, and Ł. H. Kocewiak, "Impedance-based stability analysis of voltage-controlled MMCs feeding linear AC systems," *IEEE Trans. Emerg. Sel. Topics Power Electron.*, vol. 8, no. 4, pp. 4060–4074, Dec. 2020.

[6] J. Lyu, J. Yin, H. Zhu, and X. Cai, "Impedance modeling and stability analysis of energy controlled modular multilevel converter," *IEEE Trans. Power Del.*, vol. 38, no. 3, pp. 1868–1881, Jun. 2023.

[7] J. Sun and H. Liu, "Sequence impedance modeling of modular multilevel converters," *IEEE Trans. Emerg. Sel. Topics Power Electron.*, vol. 5, no. 4, pp. 1427–1443, Dec. 2017.

[8] T. Huang, F. Yang, D. Zhang, and X. Chen, "High-frequency stability analysis and impedance optimization for an MMC-HVDC integrated system considering delay effects," *IEEE Trans. Emerg. Sel. Topics Circuits Syst.*, vol. 12, no. 1, pp. 59–72, Mar. 2022.

[9] J. Lyu, X. Zhang, X. Cai, and M. Molinas, "Harmonic state-space based small-signal impedance modeling of a modular multilevel converter with consideration of internal harmonic dynamics," *IEEE Trans. Power Electron.*, vol. 34, no. 3, pp. 2134–2148, Mar. 2019.

[10] X. Wang, L. Harnefors, and F. Blaabjerg, "Unified impedance model of grid-connected voltage-source converters," *IEEE Trans. Power Electron.*, vol. 33, no. 2, pp. 1775–1787, Feb. 2018.

[11] C. Zhang, X. Cai, A. Rygg, and M. Molinas, "Sequence domain SISO equivalent models of a grid-tied voltage source converter system for small-signal stability analysis," *IEEE Trans. Energy Convers.*, vol. 33, no. 2, pp. 741–749, Jun. 2018.

[12] C. Zhang, M. Molinas, A. Rygg, and X. Cai, "Impedance-based analysis of interconnected power electronics systems: Impedance network modeling and comparative studies of stability criteria," *IEEE Trans. Emerg. Sel. Topics Power Electron.*, vol. 8, no. 3, pp. 2520–2533, Sep. 2020.

[13] H. Gong, X. Wang, and D. Yang, "DQ-frame impedance measurement of three-phase converters using time-domain MIMO parametric identification," *IEEE Trans. Power Electron.*, vol. 36, no. 2, pp. 2131–2142, Feb. 2021.

[14] M. Zhang, X. Wang, and Q. Xu, "Data-driven modeling of power-electronics-based power system considering the operating point variation," in *Proc. IEEE Energy Convers. Congr. Expo.*, 2021, pp. 3513–3517.

[15] X. Du, J. Meng, J. Peng, Q. Peng, J. Wu, and M. Lin, "A two-stage optimization framework for fast lithium-ion battery impedance measurement," *IEEE Trans. Power Electron.*, vol. 38, no. 5, pp. 5659–5664, May 2023.

[16] T. Wang, Y. Tan, Y. Wang, B. Jin, A. Monti, and A. L. Sangiovanni-Vincentelli, "Synthetic data in DC microgrids: Label creation for ensemble learning for fault isolation," *IEEE Trans. Power Del.*, vol. 37, no. 3, pp. 2301–2313, Jun. 2022.

[17] L. Wang, Z. Qin, and P. Bauer, "A gradient-descent optimization assisted gray-box impedance modeling of EV chargers," *IEEE Trans. Power Electron.*, vol. 38, no. 7, pp. 8866–8879, Jul. 2023.

[18] M. Amin and M. Molinas, "A gray-box method for stability and controller parameter estimation in HVDC-connected wind farms based on nonparametric impedance," *IEEE Trans. Ind. Electron.*, vol. 66, no. 3, pp. 1872–1882, Mar. 2019.

[19] W. Liu, X. Xie, J. Shair, and X. Li, "A nearly decoupled admittance model for grid-tied VSCs under variable operating conditions," *IEEE Trans. Power Electron.*, vol. 35, no. 9, pp. 9380–9389, Sep. 2020.

[20] M. Nahalparvari et al., "DC-side impedance estimation of a modular multilevel converter through system identification of a partially black-boxed control system," *IEEE Trans. Energy Convers.*, vol. 37, no. 4, pp. 2708–2721, Dec. 2022.

[21] M. Zhang, X. Wang, D. Yang, and M. G. Christensen, "Artificial neural network based identification of multi-operating-point impedance model," *IEEE Trans. Power Electron.*, vol. 36, no. 2, pp. 1231–1235, Feb. 2021.

[22] M. Zhang, X. Wang, D. Yang, Z. Cui, and M. G. Christensen, "Transfer learning for identifying impedance estimation in voltage source inverters," in *Proc. IEEE Energy Convers. Congr. Expo.*, 2020, pp. 6170–6174.

[23] M. Zhang, Q. Xu, and X. Wang, "Physics-informed neural network based online impedance identification of voltage source converters," *IEEE Trans. Ind. Electron.*, vol. 70, no. 4, pp. 3717–3728, Apr. 2023.

[24] T. Roinila, M. Vilkko, and J. Sun, "Online grid impedance measurement using discrete-interval binary sequence injection," *IEEE J. Emerg. Sel. Topics Power Electron.*, vol. 2, no. 4, pp. 985–993, 2014.

[25] Y. Zhang, Y. Yang, X. Chen, and C. Gong, "Intelligent parameter design-based impedance optimization of STATCOM to mitigate resonance in wind farms," *IEEE Trans. Emerg. Sel. Topics Power Electron.*, vol. 9, no. 3, pp. 3201–3215, Jun. 2021.

[26] D. Yang, X. Wang, M. Ndreco, W. Winter, R. Juhlin, and A. Krontiris, "Automation of impedance measurement for harmonic stability assessment of MMC-HVDC systems," in *Proc. 18th Wind Integration Workshop*, 2019, pp. 1–6.

[27] S. J. Pan and Q. Yang, "A survey on transfer learning," *IEEE Trans. Knowl. Data Eng.*, vol. 22, no. 10, pp. 1345–1359, Oct. 2010.

[28] D. P. Kingma and J. Ba, "Adam: A method for stochastic optimization," in *Proc. 3rd Int. Conf. Learn. Representations*, San Diego, CA, USA, 2015. [Online]. Available: http://arxiv.org/abs/1412.6980

[29] S. Ruder, "An overview of gradient descent optimization algorithms," 2016, *arXiv:1609.04747*.

[30] X. Wang and F. Blaabjerg, "Harmonic stability in power electronic-based power systems: Concept, modeling, and analysis," *IEEE Trans. Smart Grid*, vol. 10, no. 3, pp. 2858–2870, May 2019.

Mengfan Zhang (Member, IEEE) received the B.S. and M.S. degrees in electrical engineering from the Nanjing University of Aeronautics and Astronautics, Nanjing, China, in 2015 and 2018, respectively, and the Ph.D. degree in power electronic engineering from Aalborg University, Aalborg, Denmark, in 2022.

He is currently a Postdoctoral Researcher with the KTH Royal Institute of Technology, Stockholm, Sweden. His research interests include the modeling, optimization, stability analysis, and advanced control of the power electronics dominated power systems.

Yang Zhang (Member, IEEE) received the B.S., M.S., and Ph.D. degrees in electrical engineering in 2012, 2015, and 2021, respectively, from the Nanjing University of Aeronautics and Astronautics, Nanjing, China.

From 2021 to 2023, he was an Associate Professor with the College of Electrical Engineering and Automation, Fuzhou University, Fuzhou, China. He is currently a Postdoctoral Researcher with the KTH Royal Institute of Technology, Stockholm, Sweden. His research interests include the modeling, stability analysis, and control of the power electronics-based power systems and the transportation electrification.

Qianwen Xu (Member, IEEE) received the B.Sc. degree from Tianjin University, Tianjin, China, in 2014, and the Ph.D. degree from Nanyang Technological University, Singapore, in 2018, both in electrical engineering.

From 2018 to 2020, she was a Postdoc Research Fellow with Aalborg University, Aalborg, Denmark, a Visiting Researcher with Imperial College London, London, U.K., and a Wallenberg-NTU Presidential Postdoc Fellow with Nanyang Technological University, Singapore. She is currently an Assistant Professor with the Department of Electric Power and Energy Systems, KTH Royal Institute of Technology, Stockholm, Sweden. Her research interests include advanced control, optimization, and AI application for microgrid and smart grid.

Dr. Xu is the Vice Chair for the IEEE Power and Energy Society and Power Electronics Society, Sweden Chapter, and an Associate Editor for the IEEE TRANSACTIONS ON SMART GRID, IEEE TRANSACTIONS ON TRANSPORTATION ELECTRIFICATION, and *IEEE Journal of Emerging and Selected Topics in Power Electronics*. She was a recipient of Humboldt Research Fellowship, Excellent Doctorate Research Work, Best Paper Award in IEEE PEDG 2020, Nordic Energy Award 2022, etc.